This is a "preproof" accepted article for *Journal of Glaciology*.
This version may be subject to change during the production process.
10.1017/jog.2024.100

Temporal variations in the ice volume of Xiao Dongkemadi Glacier, central Tibetan Plateau, from 1969 to 2020

An'an Chen[1,2], Ninglian Wang[1,2,3*], Zhen Li[4], Yuwei Wu[1,2] Xi Jiang[5], Zhongming Guo[1,2], Xuejiao Wu[1,2], and Xuewen Yang[1,2]

[1]Shaanxi Key Laboratory of Earth Surface System and Environmental Carrying Capacity, Northwest University, Xi'an 710127, China; [2]Qiyi Glacier Station, Institute of Earth Surface System and Hazards, College of Urban and Environmental Sciences, Northwest University, Xi'an 710127, China; [3]Institute of Tibetan Plateau Research (ITP), Chinese Academy of Sciences (CAS), Beijing 100101, China; [4]State Key Laboratory of Cryospheric Science, Northwest Institute of Eco–Environment and Resources, Chinese Academy of Sciences, Lanzhou 730000, China and [5]Joint Center for Data Assimilation Research and Applications, Nanjing University of Information Sciences and Technology(NUIST), Nanjing 210044, China

Abstract

Glaciers play a crucial role in the Asian Water Tower, underscoring the necessity of accurately assessing their mass balance and ice volume to evaluate their siginificance as sustainable freshwater resources. In this study, we analyzed ground–penetrating radar measurements from a 2020 survey of the Xiao Dongkemadi Glacier (XDG) to determine ice thickness, and we extended the glacier's volume-change record to 2020 by employing multi–source remote–sensing data. Our findings show that the GPR-derived mean ice thickness of XDG in 2020 was 54.78 ± 3.69 meters, corresponding to an ice volume of 0.0811 ± 0.0056 km^3. From 1969 to 2020, the geodetic mass balance was –0.19 ± 0.02 m w.e. a^{-1}, and the glacier experienced area and ice volume losses of 16.38 ± 4.66% and 31.01 ± 4.59%, respectively. The long–term mass balance reconstruction reveals weak fluctuations occurred from 1967 to 1993 and that overall mass losses have occurred since 1994. This ongoing shrinkage and ice loss are mainly associated with the temperature increases in the warm season since the 1960s. If the climate trend across the central Tibetan Plateau follows to the SSP585 scenario, then XDG is at risk of disappearing by the end of the century.

https://doi.org/10.1017/jog.2024.100 Published online by Cambridge University Press

1. Introduction

The Tibetan Plateau accommodates a large number of glaciers, and the meltwater from these glaciers provides valuable freshwater for the people living downstream (Immerzeel and others, 2020; Pritchard, 2019; Yao and others, 2022). Most of the glaciers across the Tibetan Plateau have experienced shrinkage and mass loss in recent decades (Brun and others, 2017; Shean and others, 2020; Yao and others, 2012; Zemp and others, 2020; Zhou and others, 2018), thereby highlighting the pressing need to accurately predict the timing of 'peak water' as global warming continues to have an ever–increasing impact on these crucial freshwater reservoirs (Gao and others, 2018; Huss and Hock, 2018). Glacier mass balance and ice volume are two key components for predicting the timing of peak water (Huss and Hock, 2018; Welty and others, 2020).

Glacier mass balance can be estimated from glaciological or geodetic methods, or on the basis of umerical modeling. The glaciological method is based primarily on stake and pit measurements, which can quantify mass balance at a high temporal resolution (Zemp and others, 2020). The geodetic method is an effective means for estimating the glacier mass balance at multiple scales (spatial and temporal) using remote–sensing–based elevation data (Brun and others, 2017; Hugonnet and others, 2021; Wu and others, 2021); however, field observations are important for verifying the glacier-scale mass balance estimates, given the uncertainties in remote–sensing data (Cogley, 2009; Xu and others, 2019). To reconstruct past and project future changes to glacier, one certainly needs a model. A variety of mass-balance modelling

https://doi.org/10.1017/jog.2024.100 Published online by Cambridge University Press

approaches are present, each with limitations, but that most require careful calibration and evaluation (Oerlemans and Reichert, 2000; Hock, 2005; Yang and others, 2013; Huss and Hock, 2015). Statistical models presume a direct relationship between glacier-wide mass balance and climate variables, and can be readily applied to glaciers with long observational records of mass balance, such as XDG. Only long–term conventional observations (temperature and precipitation) are available at the high altitude meteorological stations across the Tibetan Plateau, the statistical models used to correlate the glaciological mass balance with air temperature and precipitation is effective in reconstructing glacier mass balance in this region (Wang and others, 2010; Wang and others, 2017; Zhang and others, 2014). However, the large financial and logistical requirements of obtaining in situ field observations on the remote glaciers across the central Tibetan Plateau has resulted in continuous mass balance observations of <20 glaciers to date (WGMS, 2021; Yao and others, 2012).

Glacier thickness measurements are essential for estimating glacier volume. The ice thickness can be measured directly at full-depth boreholes to the glacier bed or via geophysical methods, including radar, seismic, geoelectric, and electromagnetic methods (Welty and others, 2020). Ground–penetrating radar (GPR), which is based on the transmission, reflection, and subsequent detection of radio waves, is the most common method (Schroeder and others, 2020). The Glacier Thickness Database v3 (GlaThiDa v3) indicates that in situ ice–thickness observations are available for only ~3000 glaciers worldwide (GlaThiDa Consortium, 2020), and <40 of these being located across the Tibetan Plateau (Cao and others, 2017; Che and others, 2022; Liu and others, 2003). Gurenhekou and Zhadang glaciers are the only glaciers in the central Tibetan Plateau with GPR–measured ice thickness constraints to date (Ma and others, 2008; Zhu and others, 2014). Due to the lack of in situ ice thickness

https://doi.org/10.1017/jog.2024.100 Published online by Cambridge University Press

measurements, the modelled ice volumes of these glaciers vary widely across this region (Bahr and others, 2015; Farinotti and others, 2019; Frey and others, 2014; Millan and others, 2022).

The Tanggula Mountains in the central Tibetan Plateau form the northern boundary of the South Asian monsoon, as defined by isotopic evidence (Tian and others, 2001; Yao and others, 2013). Systematic field investigations in the Tanggula Mountains began in 1989, with in situ glaciological measurements acquired at regular intervals across Xiao Dongkemadi Glacier (XDG) (Fujita and Ageta, 2000; Pu and others, 2008). The long–term mass balance record and field meteorological observations of XDG make it a key glacier for studying glacier–climate interactions across the central Tibetan Plateau (Fujita and Ageta, 2000; Ke and others, 2015; Liang and others, 2018; Shi and others, 2016; Zhang and others, 2013). Furthermore, shallow ice core (Li and others, 2015), albedo (Wu and others, 2015; Zhang and others, 2018), mercury deposition (Paudyal and others, 2017), ice flow velocity (Wu and others, 2016), trace elements (Li and others, 2011; Li and others, 2020), carbonaceous matter (Li and others, 2023), bacterial diversity (Xie and others, 2009), and glacier runoff (Gao and others, 2011) studies have been conducted on XDG. We have previously estimated the geodetic mass balance of the entire Tanggula Mountains (including XDG) between ~1969 and ~2015 using remote sensing data (Chen and others, 2017).

In this study, we sought to improve on the understanding of XDG volume and historic volume change. We first extended the geodetic volume change record to 2020, making use of multispectral stereoscopic satellite data, to evaluate long-term area and volume changes. Second, we conducted in situ measurements of ice thickness using a ground penetrating radar, enabling us to constrain the glacier's

https://doi.org/10.1017/jog.2024.100 Published online by Cambridge University Press

contemporary and historic volume. Finally, we reconstructed long-term mass-balance changes using a statistical model based on three decades of measurements. The field observations and remote sensing results presented in this study will enhance our understanding of the glacier variations across the central Tibetan Plateau.

2. Study area

XDG (33°10´N, 95°08´E) is located within the Dongkemadi Ice Field, Tanggula Mountains (Fig. 1). It is a small valley glacier that separated from Dongkemadi Glacier (DG) between 2000 and 2007 due to continued glacier shrinkage (Shi and others, 2016). The glacier area was 1.77 ± 0.08 km^2 in 1969, based on a topographic map, with the glacier extending from 5380 m above sea level (a.s.l.) to 5926 m a.s.l (Pu and others, 2008). Glaciological mass balance measurements have been obtained continuously since 1988/89, with the annual mass balance varying from 525 mm water equivalent (w.e.) in 1988/89 to −1066 mm w.e. in 2009/10 (Pu and others, 2008; Zhang and others, 2013). Brief weather observations from XDG during 2008–2012 indicated that the annual air temperature and precipitation near the equilibrium line were −8.6°C and 680 mm, respectively (Zhang and others, 2013).

Figure *1* near here

3. Data and methods

3.1 Mass balance during 1969–2020

3.1.1 Glaciological method

The glaciological mass balance of XDG has been monitored continuously since 1989 (Pu and others, 2008). By 2015, a network of twenty–four stakes were established to cover the entire glacier surface ranging from 5400 to 5750 m a.s.l. (Fig.

https://doi.org/10.1017/jog.2024.100 Published online by Cambridge University Press

1c). We determined the net mass balance according to the glaciological method, by measuring changes in stake heights and snowpit characteristics in both the ablation and accumulation areas. At each stake, we recorded the height of the stake above the glacier surface, snow density and thickness, presence of superimposed ice layers, and the structure of the snowpit profile (Pu and others, 2008). The mass balance at each stake is assigned to a corresponding altitude range, and the specific mass balance is depicted as a function of altitude. These measurements are then extrapolated to estimate the mass balance for the entire glacier (Chen and others, 2017). The mass balance records from 1989 to 2010 were published by Yao and others (2012), while subsequent observations have extended this record to 2016.

The mass balance derived using the glaciological method involves several sources of uncertainty, including uncertainties in field measurements at specific locations, spatial averaging of these measurements across the entire glacier, and changes in glacier area and elevation (Zemp and others, 2013). Thibert and others (2008) suggested that contributing to mass balance uncertainty—such as measurement, extrapolation, and glacier change uncertainties—can be calculated separately. Following Xu and others (2019), we estimate the uncertainty of the mass balance by 0.21 and 1.53 m w.e. for the glacier-wide and cumulative mass balance over the period from 2010 to 2016.

3.1.2 Geodetic method

The prior study of Chen and others (2017) assessed the glacier surface–elevation changes for the entirety of the Tanggula Mountains between ~1969 and ~2015. Surface elevation measurements of the glacier surface at different periods were obtained from a topographic map, Shuttle Radar Topography Mission (SRTM) 1 data,

https://doi.org/10.1017/jog.2024.100 Published online by Cambridge University Press

and Landsat Thematic Mapper/Operational Land Imager (TM/OLI), Terra Advanced Spaceborne Thermal Emission and Reflection Radiometer (ASTER), and ZiYuan–3 (ZY–3) satellite images (Table1). A Topo DEM (generated from topographic map) and ASTER DEM of XDG have previously been generated (Chen and others, 2017). We included the ZY–3 stereopsis (spatial resolution of 3.5 m) acquired on 9 October 2020 in this study to generate the ZY–3 DEM in 2020.

The Topo DEM was generated from the 1969 topographic map using the ANUDEM 5.23 software through vectorized contour lines and elevation points. The ASTER and ZY–3 DEMs were generated using the "DEM Extraction" module in ENVI 5.2. The coordinate system was defined using the datum WGS1984 UTM zone 46, and the spatial resolution was resampled to 30 m via bilinear interpolation. The SRTM approximates the surface elevation in 1999 by considering the seasonality correction (Chen and others, 2017).

Table *1* near here

The automated, iterative implementation of the co-registration algorithm for different DEMs was carried out following the method described by Nuth and Kääb (2011), and subsequently generalized by Shean and others (2016) using Python and shell scripts. The relative uncertainties of DEMs were evaluated using the non–glaciated terrain, which remained stable throughout the study period. The uncertainty in glacier elevation changes (ε_{DEM}) was calculated using Equation (1), incorporating the radar wave penetration accuracy (ε_p) and normalized median absolute deviation (NMAD, Δσ) for the glacier–free terrain after DEM co–registration (Chen and others, 2017):

$$\varepsilon_{DEM} = \sqrt{(\Delta\sigma)^2 + (\varepsilon_p)^2} \qquad (1)$$

https://doi.org/10.1017/jog.2024.100 Published online by Cambridge University Press

The relative uncertainty between Topo DEM and ZY–3 DEM can be directly described by NMAD, as both DEMs are derived from optical images. The radar wave penetration accuracy across Dongkemadi Ice Field was determined to be 3.5 m, based on comparisons of the ICESat GLA14 footprints and SRTM elevation data (Chen and others, 2017). The overall mass balance uncertainty (ε_M) was estimated using equation (2), following the methods outlined by Braun and others (2019):

$$\varepsilon_M = \sqrt{\left(\frac{\Delta M}{\Delta t}\right)^2 \left(\left(\frac{\varepsilon_{DEM}}{\Delta h}\right)^2 + \left(\frac{\varepsilon_A}{A}\right)^2 + \left(\frac{\varepsilon_\rho}{\rho}\right)^2\right) + \left(\frac{\varepsilon_p}{\Delta t} \times \rho\right)^2} \quad (2)$$

where ΔM/Δt represents the mass-balance estimate; Δh, A, and ρ (850kg m^{-3}, Huss, 2013) denote the mean elevation difference (MED) of the glacier, the glacier area and the density for volume-to-mass conversion, respectively; ε_A and ε_ρ (60kg m^{-3}, Huss, 2013) represent the uncertainties of the glacier area and conversion density, respectively.

3.2 Glacier area

XDG glacier boundaries were manually delineated using a November1969 topographic map, a Landsat–5 satellite image from 30 August 2000, and a ZY–3 satellite image from 9 October 2020. Aerial photographs from 1969 were used to produce a 1:100,000 topographic map in 1973. The map was scanned, re–projected to the Universal Transverse Mercator coordinate system, and referenced to the World Geodetic System 1984 datum. The Landsat–5 and ZY–3 satellite orthophotos have spatial resolutions of 30 and 2.1 m, respectively. The uncertainty in the glacier boundary delineated from the topographic map was set to 5%, and the uncertainties (ε_A) in the boundaries that were delineated from the satellite images were estimated by applying a half–pixel buffer to each analyzed image, as follow (Paul and others, 2013):

https://doi.org/10.1017/jog.2024.100 Published online by Cambridge University Press

$$\varepsilon_A = N \times \frac{S^2}{2} \qquad (3)$$

where N is the number of pixels of the glacier boundary and S is the spatial resolution of the image. The uncertainty in the glacier area change(ε_{AC}) for each pair of images was calculated based on error propagation (Guo and others, 2013), as follows:

$$\varepsilon_{AC} = \sqrt{\varepsilon_{A1}^2 + \varepsilon_{A2}^2} \qquad (4)$$

where ε_{A1} and ε_{A2} represent the uncertainties of the glacier area of each image.

3.3 GPR measurements and glacier volume

A GPR survey was conducted on XDG in August 2020 using a pulseEKKO PRO system to constrain the ice thickness of the glacier. A total of 122 GPR measurements were obtained along one longitudinal profile and six transverse profiles (Fig. 2a), with measurement spacings of approximately 30 and 40 m, respectively. The GPR operated at a frequency of 100 MHz, with the transmitting and receiving antennas separated by 1.5 meters at each measurement point. The radargrams clearly showed the glacier bedrock interface for each profile (Fig. 2b), and the ice thickness was calculated based on the two–way travel time of the GPR reflection from glacier bedrock interface, using a radio–wave velocity of 0.169 m ns^{-1} for glacier ice. The GPR measurement locations were surveyed with a Unistrong MG868 global positioning system (GPS), which provides single point positioning accuracy of 1.2 m. The same GPR parameters were employed at Bayi Glacier, where a 1% uncertainty was reported between the measured ice thickness and ice core length through the glacier (Wang and Pu, 2009). The ice thickness data were interpolated using the Ordinary Kriging method and constrained by glacier outline to create an ice thickness raster. This raster was

https://doi.org/10.1017/jog.2024.100 Published online by Cambridge University Press

subsequently used to calculate the mean ice thickness and ice volume of XDG over the five–decade analysis period.

Figure *2* near here

We created a glacier bed DEM for XDG by subtracting the 2020 GPR derived ice thickness raster from the 2020 ZY–3 DEM. Using this glacier bed DEM, we calculated the elevation differences between the glacier bed DEM and the 1969 topographic map, the 2000 SRTM, and the 2015 ASTER DEM to estimate ice thicknesses for 1969, 1999, and 2015, respectively. By combining these ice thickness estimates with the glacier area at different times, we reconstructed the corresponding ice volumes for XDG. The DEM projections were transformed to the WGS1984/UTM zone 46 coordinate system, and their spatial resolutions were resampled to 30 m.

The uncertainties in both the glacier area (ε_A) and mean ice thickness ($\varepsilon_{\bar{H}}$) are needed to assess the glacier volume uncertainty (ε_V) as follows:

$$\varepsilon_V = \sqrt{(\bar{H} \times \varepsilon_A)^2 + (A \times \varepsilon_{\bar{H}})^2} \quad (5)$$

The uncertainty in the glacier area is detailed in Section 3.2, A is glacier area. The uncertainty in ice volume change (ε_{VC}) for each period was calculated using error propagation methods:

$$\varepsilon_{VC} = \sqrt{(MED \times \varepsilon_A)^2 + (A_F \times \varepsilon_{DEM})^2} \quad (6)$$

where A_F and ε_A represent the glacier area and the uncertainty of glacier area at former time in each period. The MED and ε_{DEM} are detailed in Section 3.1. The uncertainties of reconstructed ice thicknesses ($\varepsilon_{\bar{H}}$) are the uncertainty in glacier elevation changes (ε_{DEM}) between glacier bed DEM and multi-temporal DEMs. The uncertainty in the ice thickness ($\varepsilon_{\bar{H}}$) derived from GPR measurements is divided into two components: the GPR measurement uncertainty (ε_{Hdata}) and the uncertainty

https://doi.org/10.1017/jog.2024.100 Published online by Cambridge University Press

associated with the Ordinary Kriging method results (ε_{HRMSE}) (Che and others, 2022):

$$\varepsilon_{\bar{H}} = \sqrt{\varepsilon_{Hdata}^2 + \varepsilon_{HRMSE}^2} \quad (7)$$

The GPR measurement uncertainty (ε_{Hdata_i}) is influenced by the pulsed–radar measurement uncertainty (ε_{HGPR_i}) and the horizontal positioning uncertainty (ε_{Hxy_i}). Consequently, the ice thickness uncertainty at each measurement point can be estimated as follows (Lapazaran and others, 2016):

$$\varepsilon_{Hdata_i} = \sqrt{\varepsilon_{HGPR_i}^2 + \varepsilon_{Hxy_i}^2} \quad (8)$$

We estimate the uncertainty in the mean ice thickness (ε_{Hdata}) of entire glacier as the average of the uncertainties from all the GPR measurement points:

$$\varepsilon_{Hdata} = \frac{1}{n}\sqrt{\sum_{i=1}^{n} \varepsilon_{Hdata_i}^2} \quad (9)$$

The horizontal positioning uncertainty is determined by the GPS accuracy (1.2 m) because the GPS was not directly linked to the GPR in the field. The pulsed–radar measurement uncertainty (ε_{HGPR}) is derived from the uncertainties in the radio wave velocity in ice (ε_{H_c}) and the observed travel time (ε_{H_t}), as follows:

$$\varepsilon_{HGPR} = \sqrt{\varepsilon_{H_c}^2 + \varepsilon_{H_t}^2} \quad (10)$$

where $\varepsilon_{H_c} = (\varepsilon_c \times t)/2$ and $\varepsilon_{H_t} = (\varepsilon_t \times c)/2$ are the components of the thickness uncertainty due to uncertainties in the radio wave velocity in ice and the observed travel time (ε_t) respectively. Here, *t* and *c* represent the time and velocity of the radar signal in ice, respectively. We assume $c = 0.169\ m \cdot \mathrm{n}s^{-1}$, $\varepsilon_c = 0.02c$, and $\varepsilon_t = 1/f_r$, where f_r is the frequency of the GPR (100 MHz in this study).

We used 85% of the measured points for interpolation and reserved the remaining 15% for cross–validation. These cross–validation points were randomly distributed across the entire glacier to quantitatively assess uncertainties in the

https://doi.org/10.1017/jog.2024.100 Published online by Cambridge University Press

interpolation method (Fig. 3a). The uncertainty in the Ordinary Kriging method results (ε_{HRMSE}) is represented by the root mean square error (RMSE), calculated from the interpolated ($\widehat{y_i}$) and measured (y_i) ice–thickness values:

$$\varepsilon_{HRMSE} = \sqrt{\frac{(y_1-\widehat{y_1})^2+(y_2-\widehat{y_2})^2+\cdots+(y_i-\widehat{y_i})^2}{i}} \quad (11)$$

The cross–validation test revealed an RMSE of 3.31 m between interpolated and measured ice thicknesses (Fig. 3b). The high consistency with an R^2 value of 0.99, indicates that the ice thickness estimates for XDG using the Ordinary Kriging method are reliable.

Figure *3* near here

3.4 Meteorological Data

Anduo meteorological station (32°21′N, 91°06′E, 4800 m) is located on the southern slope of the Tanggula Mountains (Fig. 1a), and is the closest station (121 km) to XDG. We selected meteorological data from Anduo station to investigate the potential drivers behind the observed variations in XDG's mass balance. Temperature and precipitation data were provided by the Chinese National Meteorological Center (http://data.cma.cn/site/index.html). The average annual temperature and precipitation over the long-term period from 1967 to 2020 are –2.4°C and 447.6 mm, respectively.

To better understand the meteorological conditions at XDG, we assessed the climatic elements at the median elevation of 5600 m (Fig. 4). This analysis is based on observational data from Anduo station and the altitudinal gradients for the warm season:–0.63 ^{o}C/100 m for temperature (Shi and others, 2020) and 23 mm/100 m for precipitation (Zhang and others, 2013).

Figure *4* near here

https://doi.org/10.1017/jog.2024.100 Published online by Cambridge University Press

Considering the differences in the extent to which glaciological mass balance is influenced by temperature and precipitation in different periods of the year, it is necessary to select a reasonable period of the year when there is a significant correlation between the temperature and/or precipitation and glacier mass balance. The climate data were therefore divided into several seasonal periods: cold season (October to April), warm season (May to September), winter (December to February) and summer (June to August) (Pu and others, 2008). We will identify the climatic factors most strongly correlated with glacier mass balance to serve as the key drivers in constructing the statistical model.

3.5 Statistical model of glacier mass balance

Given that the statistical model is effective for reconstructing mass balance using only conventional meteorological data (Wang and others, 2010), we select this approach to reconstruct the mass-balance history of XDG over the past 50 years. A correlation model between glacier mass balance and climatic factors for XDG is established by using the 28–year times series of XDG mass balance observations and the long–term climate data at the median elevation of XDG. This method enabled us to reconstruct past mass-balance variations and assess the sensitivity of the glacier mass balance to climate change. We constructed a multivariate regression based on the correlation analysis results in section 4.4, with the temperature and precipitation as independent variables and glacier mass balance as the dependent variable. We chose to assess the uncertainty of reconstructed mass balances (ε_{RM}) by constructing confidence intervals of them (He and Liu, 2015), as follows:

$$\varepsilon_{RM} = z_{\alpha/2} \times SE \qquad (12)$$

where α is the significance level, and the value of the statistical model is used in

https://doi.org/10.1017/jog.2024.100 Published online by Cambridge University Press

this paper, $z_{\alpha/2}$ is the two-sided quantile of the standard normal distribution, which can be obtained by looking up the standard normal distribution table. SE is the standard error of the reconstructed mass balance.

4. Results

4.1 Geodetic and glaciological mass balances of XDG

Figure 5 shows the annual (blue) and cumulative (red) mass balance for 1989–2016, as calculated using the glaciological method. The cumulative glaciological mass balance of XDG was –8.47 ± 1.53 m w.e., and the annual mass balance varied between +0.52 ± 0.21 and −1.07 ± 0.21 m w.e. a^{-1}, with a mean of −0.30 ± 0.21 m w.e. a^{-1} over the 28–year period. We extended the XDG mass-balance time series to 2020 by combining the results of this study with those from our previous research (Chen and others, 2017, Fig. 5, Table 2). XDG experienced continued mass loss from 1969 to 2020, with a cumulative geodetic mass balance of −9.69 ± 3.06 m w.e., equivalent to an annual rate of –0.19 ± 0.02 m w.e. a^{-1}. The mass loss varied over different periods: limited loss of –0.06 ± 0.10 m w.e. a^{-1} from 1969 to 1999, an increased rate of –0.41 ± 0.14 m w.e. a^{-1} from 1999 to 2015 (which is close to the glaciological value of -0.42± 0.21 m w.e. a^{-1}), and –0.32 ± 0.14 m w.e. a^{-1} from 2015 to 2020.

Figure 5 near here
Table 2 near here

4.2 Glacier area changes during 1969–2020

https://doi.org/10.1017/jog.2024.100 Published online by Cambridge University Press

The changes in the ice–covered area of XDG from 1969 to 2020, based on comparisions between the 1969 topographic map and the 1999, 2015, and 2020 satellite images (Fig. 6, Table 2), show a decrease from 1.77 ± 0.08 to 1.48 ± 0.02 km^2, amounting to a reduction of 0.29 ± 0.08 km^2 (16.38 ± 4.66%). XDG has experienced continuous shrinkage throughout the different investigated periods, with the highest annual shrinkage rate of –0.64 ± 0.52% a^{-1} occurring between 1999 and 2015. The loss is primarily due to the retreat of the glacier terminus and surface lowering at the western headwall (indicated by the orange circle in Fig. 6).

Figure *6* near here

4.3 Glacier thickness in 2020 and ice volume changes during 1969–2020

We interpolated measurements from 104 GPR points to calculate the thickness of XDG. In 2020, the glacier had a mean ice thickness of 54.78 ± 3.69 m, with the thickest ice (146.88 ± 1.69 m) found in the upper firn basin. The thickness distribution indicates a gradual increase from the glacier edges toward the central part (Fig. 7a). Along this central part, the ice thickness exceeds 120 m for approximately half of the glacier's length, with the maximum thickness occurring in the upper firn basin, where it surpasses 135 m (Fig. 6a). The glacier bed's topography resembles that of a typical valley (Fig. 7b), showing an increasing breadth–depth ratio with higher elevations.

Figure *7* near here

In 2020, XDG had an ice volume of 0.0811 ± 0.0056 km^3, calculated from a mean ice thickness of 54.78 ± 3.69 m and a glacier area of 1.48 ± 0.02 km^2. The reconstructed ice volumes for XDG were 0.1175 ± 0.0066 in 1969, 0.1073 ± 0.0104 in 1999, and 0.0848 ± 0.0047 km^3 in 2015, as determined from topographic map, SRTM,

https://doi.org/10.1017/jog.2024.100 Published online by Cambridge University Press

and ASTER DEM, respectively. These volumes corresponded to mean ice thicknesses of 66.40 ± 3.44, 64.28 ± 3.73, and 56.56 ± 2.13 m, respectively (Table 3). Surface elevation change maps (Fig. 8) indicate that XDG has experienced ice loss throughout all investigated periods, with a total loss of 0.0364 ± 0.0051 km^3 (31.01 ± 4.59%) over from 1969 to 2020. The ice loss rate was 0.29 ± 0.18 %·a^{-1} from 1969 to 1999, which is much lower than the rates of 1.00 ± 0.37 and 0.89 ± 0.75 %·a^{-1} during 1999–2015 and 2015–2020, respectively.

Figure *8* near here

Table 3 near here

4.4 Statistical mass balance reconstruction from 1967 to 2020

To identify the optimal climate factors for driving the statistical model of glacier mass balance, we analyze the correlation coefficients between the XDG mass balance and temperature and precipitation data from Anduo station from the period 1989–2016 (Table 4). The correlation coefficients between mass balance and temperature were approximately −0.79 ($p < 0.01$) for both the warm season and summer. Given that glacier melting at XDG typically begins in May, we selected the temperature during the warm season as a key climatic factor influencing the glacier's mass balance. Significant correlations were found between the mass balance and precipitation during both the annual and warm seasons (Table 4). Over 90% of the precipitation in the Dongkemadi basin falls during the warm season (He and others, 2009), and recent field observations show minimal mass change during the cold season (October to April). Consequently, we consider warm season precipitation as an additional key climatic factor affecting glacier mass balance.

https://doi.org/10.1017/jog.2024.100 Published online by Cambridge University Press

Table *4* near here

To reconstruct and predict the mass balance of XDG, we used multivariate regression to determine the relationship between the mass balance (M_b, mm w.e.), warm season temperature (T_w, °C), and precipitation (P_w, mm) at the median glacier height as follows:

$$M_b = -498.1 \times T_w + 1.1 \times P_w - 399.6 \ (R^2=0.65, n=28) \quad (13)$$

The variance test of the regression formula showed that the significance level was within 0.01, indicating a strong relationship between the parameters. The uncertainty of the reconstructed mass balances, calculated using Equation (12), was 0.12 m w.e.. The reconstructed mass balance of XDG ranged from −0.82 to +0.44 m w.e., with a long-term average of −0.20 ± 0.12 m w.e., over the period from 1967 to 2020. The cumulative mass balance during this time was –10.60 m w.e., indicating mass loss during this period (Fig. 9a). The mass balance reconstruction shows that XDG experienced two distinct patterns of change during 1967–2020, the mass balance exhibited weak fluctuations from 1967 to 1993 (with the cumulative mass balance of –0.15 m w.e.), and overall mass losses have occurred since 1994 (with the cumulative mass balance of –10.45 m w.e.). This pattern aligns with similar observations reported by Shangguan and others (2008), and Zemp and others, (2020) documented a comparable trend of negative glacier mass balance on a global scale.

Figure *9* near here

5. Discussion

5.1 Validation of the mass balance estimates from different methods

https://doi.org/10.1017/jog.2024.100 Published online by Cambridge University Press

Mass balance is a basic parameter for monitoring glacier changes. We estimated the mass balance of XDG by using glaciological methods, geodetic methods, and statistical models. The glaciological method is a widely accepted approach for measuring mass balance, and the glaciological mass balance is used to verify the mass balance acquired from other methods. We had verified the good agreement between glaciological and geodetic mass balances of XDG, and the absolute differences in mass balances between the two methods were <5% for the different periods between 1999 and 2015 (Chen and others, 2017). For the period of 1989–2016, the reconstructed cumulative mass balance of –8.17 m w.e. closely matches the glaciological value of –8.47 ± 1.53 m w.e., and the correlation coefficient between reconstructed and glaciological values was 0.80 (RMSE=0.25, $p < 0.01$, Fig. 9b). The reconstructed mean mass balances were –0.21± 0.12, –0.08± 0.12, –0.34± 0.12, and –0.58± 0.12 m w.e.a^{-1} for the periods of 1969–2020, 1969–1999, 1999–2015 and 2016–2020, respectively. These values are approximate to the geodetic mass balances of –0.19 ± 0.02, –0.06 ± 0.10, –0.41 ± 0.14, and –0.32 ± 0.14 m w.e. a^{-1} for the corresponding periods. The verification results show that the mass balances of XDG estimated by different methods have good agreement, which gives us the confidence to compare with others.

5.2 Comparison of glacier variations with other studies

Remote sensing data have documented significant glacier shrinkage across the Tibetan Plateau, particularly in its central part. Previous studies have focused on regional-scale glacier changes, noting a 28.94% reduction in glaciers across the Tanggula Mountains between 1980 and 2020 (Zhang, 2023) and a surface elevation

https://doi.org/10.1017/jog.2024.100 Published online by Cambridge University Press

change of –0.36 ± 0.06 m a^{-1} between ~1969 and 2015 (Chen and others, 2017). A GPS survey conducted on XDG in October 2007 indicated a surface lowering rate of 0.21± 0.14 m a^{-1} between 1969 and 2007 (Shangguan and others, 2008). This rate falls between the surface-lowering rates observed for the 1969–1999 and 1999–2015 periods in this study. Hugonnet and others (2021) provided mass balance time series of DG, which includes Dadongkema Glacier and XDG (Figure 1 and Table 5). Their study calculated a mass balance of –0.87±0.46 m w.e. a^{-1} for 2015–2020, which is higher than the geodetic result of –0.32 ± 0.14 m w.e. a^{-1} for the same period in this study. There were three possible reasons for the discrepancy between these two studies. First, the calculation methods differ. We computed glacier elevation changes by differencing DEMs from two distinct epochs, while Hugonnet and others (2021) derived elevation changes from time series data and interpolated elevation observations into continuous time series using Gaussian process regression. Secondly, the specific time period of the geodetic mass balance from Hugonnet and others (2021) is from January 1, 2015 to January 1, 2020, corresponding mass-balance year is from 2014/2015 to 2018/2019 after considering the seasonality correction. For our geodetic mass balance, the corresponding mass-balance year is from 2015/2016 to 2019/2020. The reconstructed records indicated that the mass loss in 2014/2015 (-0.80 m w.e. a^{-1}) was approximately twice that in 2019/2020 (-0.42 m w.e. a^{-1}). The third possible reason is different pixel resolutions between Hugonnet and others (2021, 100 m) and our study (30 m). The comparison of annual mass balance revealed a RMSE of 0.30 m w.e. between the glaciological method of XDG and that of Hugonnet and others (2021) for the period of 2000-2016 (Fig. 10). The weak consistency (R^2=0.34) of two datasets between the datasets suggests that the regional ASTER data have

https://doi.org/10.1017/jog.2024.100 Published online by Cambridge University Press

limitations for estimating annual mass-balance, but better consistency observed over five-year and decade scales (Table 5).

Figure *10* near here
Table 5 near here

5.3 Comparison between gridded and observed ice thickness

Accurate assessments of a glacier's ice volume and thickness distribution are critical for evaluating its water resource potential and predicting glacier variations. Based on multi–source DEMs, Farinotti and others (2019), and Millan and others (2022) estimated the global ice thickness using a weighted ensemble of five models and shallow-ice approximation, respectively. They shared the gridded products, which significantly enhanced the understanding of the distribution of global ice thickness. However, the gridded products of central Asia released by Millan and others (2022) were most likely calculated from the GDEM, but the acquisition time of GDEM is unclear. Farinotti and others (2019) estimate the ice volume of XDG as 0.1061 km^3, based on SRTM data for the Tibetan Plateau. This value is close to the reconstructed ice volume of 0.1073 ± 0.0104 km^3 for 1999 in this study. However, the glacier thickness distribution released by Farinotti and others (2019) shows thinner ice in the middle and thicker ice near the edges compared to the reconstructed and observed ice thicknesses in 1999 (Figure 11a) and 2020 (Figure 7a), respectively. Additionally, the thickest ice of XDG in the gridded products of Farinotti and others (2019) was recorded as 104.37 m in 1999, which is approximately 42 m less than the observed maximum thickness in 2020. These discrepancies in ice thickness distribution and the maximum ice thickness suggest that additional glacier measurements in the Tibetan Plateau are necessary to refine and improve the accuracy of existing glacier thickness

https://doi.org/10.1017/jog.2024.100 Published online by Cambridge University Press

products.

Figure *11* near here

Ice thickness measurements for glaciers across the Tibetan Plateau are limited due to their remote locations, and the available measurements carry a high degree of uncertainty. The uncertainty in ice thickness is divided into two components: GPR measurement uncertainty and interpolation method uncertainty. GPR measurement uncertainty is a systematic error, and can be quantitatively assessed using specific equations (Lapazaran and others, 2016). In contrast, uncertainties in estimating the thickness of the entire glacier are primarily influenced by the interpolation methods used, which depend on the number and distribution of measurement points. Langhammer and others (2019a) employed elements of sequential optimized experimental design (SOED) for determining cost-optimized GPR survey layouts, but their results were difficult to offer general recommendations. When high-precision ice thickness maps are required, it is therefore advisable to acquire as much data as can be afforded (Langhammer and others, 2019a). However, ground-based GPR measurements on glacier often struggle to capture ice thicknesses at the upper regions and edges due to accessibility issues, yet these areas are crucial for estimating the overall glacier thickness. The advancement of helicopter-borne GPR presents a significant opportunity for more comprehensive ice thickness surveys, greatly enhancing the quantity and coverage of measurements. Since the first study reported by Kennett and others (1993), helicopter-borne ice thickness measurements of several alpine glaciers have been completed (Blindow and others, 2012; Langhammer and others, 2019b). Pritchard and others (2020) developed the Bedmap Himalayas airborne radar system mainly based on an airborne ice-sounding radar, with which successful experiments were conducted on several glaciers in Nepal. It is believed that

https://doi.org/10.1017/jog.2024.100 Published online by Cambridge University Press

the airborne ice-sounding radar will be applied to the ice thickness measurement in the central Tibet Plateau in the near future, which will provide an effective means for obtaining accurate ice thickness information.

5.4 Mass balance models of XDG

XDG has the longest record in the central Tibetan Plateau, making it an excellent test location for various glacier mass balance models. A distributed temperature–index mass balance model coupled with volume–area scaling method has previously been applied for predicting variations of XDG and Dongkemadi Ice Field in the future (Shi and others, 2020; Shi and others, 2016). Liang and others (2018) developed a modified distributed surface energy–balance model (DSEBM) with high spatial–temporal resolution, which has been employed to reconstruct the mass balance of the DG from 1960 to 2009 and to analyze its influencing factors (Liang and others, 2019; 2020; 2022). Recently, a hybrid modelling approach has been introduced, coupling an empirical glacier evolution model with a temperature–index model to project response of DG to climate change through 2100 (Han and others, 2023). Compared with the sophisticated models mentioned above, the statistical mass balance model offers advantages such as lower input requirements (limited to temperature and precipitation) and ease of calculation, making it an effective tool for reconstructing glacier mass balance on the Tibetan Plateau (Wang and others, 2010; Wang and others, 2017; Zhang and others, 2014). The reconstructed cumulative mass balance of XDG, calculated using the statistical mass balance model, was −4.65 m w.e. for the period of 1967–2009, which was similar to the value for DG (-5.45 m w.e., calculated using the DSEBM) over the same period (Liang and others, 2019). However, the model does not account for the dynamic evolution of glacier morphology, limiting its

https://doi.org/10.1017/jog.2024.100 Published online by Cambridge University Press

ability to project future glacier variations.

The statistical model indicated a mass balance sensitivity of XDG to warm season temperature and precipitation of –498 mm w.e./^{o}C and +1.1 mm w.e./1 mm, respectively. A similar analysis result for Urumqi Glacier No. 1 suggested that a 1 ^{o}C increase in summer temperature led to a 441 mm w.e. decrease in glacier mass balance, while a 1 mm increase in annual precipitation led to a 1.2 mm w.e. increase in glacier mass balance (Zhang and others, 2014). Wang and others (2017) reported that the mass balance sensitivity to air temperature for Qiyi Glacier in the Qilian Mountains was –239 mm w.e./^{o}C, while the sensitivity to the precipitation was +1.1 mm w.e. per 1 mm increase. These studies reveal that while mass balance sensitivity to air temperature varies across regions on the Tibetan Plateau, the sensitivity to precipitation remains consistent. Previous studies have reported that the effects of a 1 °C warming on the mass balance were equivalent to a >25% increase in precipitation (Oerlemans, 2005; Wang and others, 2017; Zhang and others, 2014). Linear–fitting results reveal a significant increase in the warm season temperature (0.27°C 10 a^{-1}, $p<0.01$) and a slight increase in the warm season precipitation (11.15 mm 10 a^{-1}; equivalent to 1.87% 10 a^{-1}) at the median height of XDG during 1967–2020 (Fig 4), which explained the ongoing shrinkage and ice loss of the glacier since the 1960s.

Han and others (2023) predicted that by 2100, the ice volume of DG will be reduced to just 3% of its 2018 level under the SSP585 scenario, which aligns with the projected ~95% ice loss across the entire Tanggula Mountains under the RCP8.5 scenario using the Python Glacier Evolution Model (Rounce and others, 2020). Both studies utilized ice thickness data from Farinotti and others (2019). However, the overestimated ice thickness near the edges of XDG in the gridded products of

https://doi.org/10.1017/jog.2024.100 Published online by Cambridge University Press

Farinotti and others (2019) may lead to a slower rate of recent glacier shrinkage, while the underestimated thickness in the middle part of glacier suggests that it will retain less ice by 2100. Nevertheless, with anthropogenic warming already at 1.25°C above the 1850-1900 baseline and expected to exceed 1.5°C within the next decade (Matthews and Wynes, 2022), the Tibetan Plateau climate is likely to follow the SSP585 scenario for the rest of this century. This indicates that XDG is at risk of disappearing before 2100. Future work needs to undertake a more sophisticated glacier evolution projection using the refined understanding of XDG ice thickness and mass balance.

6. Conclusions

As one of the alpine glaciers with the longest continuous mass-balance observational record in the central Tibetan Plateau, XDG serves as a key indicator for understanding how glaciers in this region may evolve in a warming global climate. This study documented the overall shrinkage and ice loss of XDG from 1969 to 2020 using a combination of field observations and remote sensing techniques. During this period, the ice–covered area of XDG decreased from 1.77 ± 0.08 km^2 in 1969 to 1.48 ± 0.02 km^2 in 2020, with a corresponding ice volume loss of 0.0364 ± 0.0051 km^3, equivalent to 31.01 ± 4.59% of the 1969 ice volume. By 2020, the mean ice thickness of XDG was measured at 54.78 ± 3.69 m, translating to an ice volume of 0.0811 ± 0.0056 km^3. Although the ice volume of XDG in GlaThiDa v3 closely matched the reconstructed value, there were obvious discrepancies in the distribution of ice thickness and location of thickest ice. Enhancing the accuracy of the glacier thickness estimates requires increasing the number and coverage of measurements, which underscores the need for broader adoption of airborne ice-sounding radar technology.

https://doi.org/10.1017/jog.2024.100 Published online by Cambridge University Press

Continuous field observations at XDG indicated that the mean annual mass balance was −0.30 ± 0.21 m w.e. for the period from 1989 to 2016, with records extended to the 2015–2020 period through geodetic methods, showing a value of –0.32 ± 0.14 m w.e.. Long–term mass balance reconstructions using statistical models indicate a cumulative mass balance of –10.60 m w.e., averaging −0.20 ± 0.12 m w.e. from 1967 to 2020. The year 1993 marked a turning point in mass-balance trends, with relatively stable conditions up to that point, followed by significant ice loss thereafter. Warming temperatures have been the dominant driver of shrinkage and ice loss of XDG since the 1960s. XDG faces the risk of disappearing before 2100 if the climate scenario of Tibetan Plateau toward to SSP585 scenario.

Acknowledgmemts. We thank the Scientific Editor Evan Miles, the Associate Chief Editor Nicolas Eckert, and the anonymous reviewers for their constructive comments. This work is supported by the Second Tibetan Plateau Scientific Expedition and Research Program (No. 2019QZKK020102), the National Natural Science Foundation of China (No. 42130516, 42171139, 41871053), Natural Science Basic Research Program of Shaanxi Province (No. 2023–JC–QN–0300), and the Qin Chuangyuan Innovation and Entrepreneurship Talent Project (No. QCYRCXM-2023-096).

Author contributions. Ninglian Wang and An'an Chen designed the study, An'an Chen led data analysis and drafted the manuscript. Zhen Li, Yuwei Wu and An'an Chen carried out field investigations and data collection. Xi Jiang, Zhongming Guo, Xuejiao Wu, and Xuewen Yang were involved in the discussions. All authors discussed results, implications, provided feedback and approved of the final manuscript.

https://doi.org/10.1017/jog.2024.100 Published online by Cambridge University Press

Data availability. The mass balance observations and ice thickness measurements were provided by Qiyi Glacier Station and access can be granted upon request by contacting the corresponding author.

References

Bahr DB, Pfeffer WT and Kaser G (2015) A review of volume-area scaling of glaciers. *Reviews of Geophysics* **53**(1)**,** 95-140. doi: 10.1002/2014rg000470

Blindow N, Salat C and Casassa G (2012) Airborne GPR sounding of deep temperate glaciers–Examples from the Northern Patagonian Icefield. In Ground Penetrating Radar (GPR), *2012 14th International Conference on*, pp. 664–669. doi: 10.1109/ICGPR.2012.6254945.

Braun MH and 8 others (2019) Constraining glacier elevation and mass changes in South America. *Nature Climate Change* **9**(2)**,** 130-136. doi: 10.1038/s41558-018-0375-7

Brun F, Berthier E, Wagnon P, Kääb A and Treichler D (2017) A spatially resolved estimate of High Mountain Asia glacier mass balances from 2000 to 2016. *Nature Geoscience* **10**(9)**,** 668-673. doi: 10.1038/ngeo2999

Cao B, Pan BT, Guan WJ, Wang J and Wen ZL (2017) Changes in ice volume of the Ningchan No. 1 Glacier, China, from 1972 to 2014, as derived from in situ measurements. *Journal of Glaciology* **63**(242)**,** 1025-1033. doi: 10.1017/jog.2017.70

Che Z, Wang NL, Liang Q and Chen AA (2022) Analysis of ice thickness sounded by ground penetrating radar and ice volume of Tuolainanshan Glacier No. 6 in the

Qilian Mountains. *Journal of Glaciology and Geocryology* **44**(5)**,** 1409-1418 (in Chinese). doi: 10.7522/j.issn. 1000–0240.2022.0127

Chen AA, Wang NL, Li Z, Wu YW, Zhang W and Guo ZM (2017) Region-wide glacier mass budgets for the Tanggula Mountains between ~1969 and ~2015 derived from remote sensing data. *Arctic Antarctic and Alpine Research* **49**(4)**,** 551-568. doi: 10.1657/aaar0016-065

Cogley JG (2009) Geodetic and direct mass-balance measurements: comparison and joint analysis. *Annals of Glaciology* **50**(50)**,** 96-100. doi: 10.3189/172756409787769744

Farinotti D and 7 others (2019) A consensus estimate for the ice thickness distribution of all glaciers on Earth. *Nature Geoence* **12,** 168-173. doi: 10.1038/s41561-019-0300-3

Frey H, and 9 others (2014) Estimating the volume of glaciers in the Himalayan-Karakoram region using different methods. *The Cryosphere* **8**(6)**,** 2313-2333. doi: 10.5194/tc-8-2313-2014

Fujita K and Ageta Y (2000) Effect of summer accumulation on glacier mass balance on the Tibetan Plateau revealed by mass-balance model. *Journal of Glaciology* **46**(153)**,** 244-252. doi: 10.3189/172756500781832945

Gao HK, He XB, Ye BS and Gao X (2011) The Simulation of HBV Hydrology Model in the Dongkemadi River Basin, Headwater of the Yangtze River. *Journal of Glaciology and Geocryology* **33**(1)**,** 171-181 (in Chinese). doi: 10.7522/j.issn.1000–0240(2011)01–0171–11

Gao HK, Li H, Duan Z, Ren Z, Meng XY and Pan XC (2018) Modelling glacier variation and its impact on water resource in the Urumqi Glacier No. 1 in Central

Asia. *Science of the Total Environment* **644,** 1160-1170. doi: 10.1016/j.scitotenv.2018.07.004

GlaThiDa Consortium (2020) Glacier Thickness Database 3.1.0. World Glacier Monitoring Service. Zurich, Switzerland. doi: 10.5904/wgms-glathida-2020-10

Guo WQ, Liu SY, Wei JF and Bao WJ (2013) The 2008/09 surge of central Yulinchuan glacier, northern Tibetan Plateau, as monitored by remote sensing. *Annals of Glaciology* **54**(63)**,** 299-310. doi: 10.3189/2013AoG63A495

Han PF, Long D, Zhao FY and Slater LJ (2023) Response of Two Glaciers in Different Climate Settings of the Tibetan Plateau to Climate Change Through Year 2100 Using a Hybrid Modeling Approach. *Water Resources Research* **59,** e2022WR033618. doi: 10.1029/2022wr033618

He XB, Ye BS and Ding YJ (2009) Bias correction for precipitation mesuament in Tanggula Mountain Tibetan Plateau. *Advances in Water Science* **20**(3)**,** 403-408 (in Chinese). doi: 10.14042/j.cnki.32.1309.2009.03.01

He XQ and Liu WQ (2015) Applied Regression Analysis (Fourth Edition). Beijing, China Renmin University Press (in Chinese).

Hock R (2005) Glacier melt: a review of processes and their modelling. *Progress in Physical Geography-Earth and Environment* **29**(3)**,** 362-391. doi: 10.1191/0309133305pp453ra

Hugonnet R and 10 others (2021) Accelerated global glacier mass loss in the early twenty-first century. *Nature* **592**(7856)**,** 726-731. doi: 10.1038/s41586-021-03436-z

Huss M (2013) Density assumptions for converting geodetic glacier volume change to mass change. *The Cryosphere* **7**(3)**,** 877-887. doi: 10.5194/tc-7-877-2013

Huss M and Hock R (2015) A new model for global glacier change and sea-level rise. *Frontiers in Earth Science* **3,** 54. doi: 10.3389/feart.2015.00054

Huss M and Hock R (2018) Global-scale hydrological response to future glacier mass loss. *Nature Climate Change* **8**(2)**,** 135-140. doi: 10.1038/s41558-017-0049-x

Immerzeel WW and 31 others (2020) Importance and vulnerability of the world's water towers. *Nature* **577**(7790)**,** 364-369. doi: 10.1038/s41586-019-1822-y

Ke LH, Ding XL and Song CQ (2015) Estimation of mass balance of Dongkemadi glaciers with multiple methods based on multi-mission satellite data. *Quaternary International* **371,** 58-66. doi: 10.1016/j.quaint.2015.02.043

Kennett M, Laumann T and Lund C (1993) Helicopter-borne radioecho sounding of Svartisen, Norway. *Annals of Glaciology*, **17**, 23–26. doi:10.3189/S0260305500012568

Langhammer L, Grab M, Bauder A and Maurer H (2019a) Glacier thickness estimations of alpine glaciers using data and modeling constraints. *The Cryosphere* **13**(8), 2189-2202. doi: 10.5194/tc-13-2189-2019

Langhammer L and 6 others (2019b) Glacier bed surveying with helicopter-borne dual-polarization ground-penetrating radar. *Journal of Glaciology* **65**(249), 123-135. doi: 10.1017/jog.2018.99

Lapazaran JJ, Otero J, Martin-Espanol A and Navarro FJ (2016) On the errors involved in ice-thickness estimates I: ground-penetrating radar measurement errors. *Journal of Glaciology* **62**(236)**,** 1008-1020. doi: 10.1017/jog.2016.93

Li Q, Wang NL, Wu XB, Pu JC, Zhang CW and He JQ (2011) Environmental Records within the Snowpits in the Yuzhufeng Glacier and Xiao Dongkemadi Glacier on the Tibetan Plateau. *Journal of Glaciology and Geocryology* **33**(1)**,** 47-54 (in Chinese). doi: 10.7522/j.issn.1000–0240(2011)01–0047–08

Li XF and 9 others (2023) Concentrations, sources, fluxes, and absorption properties

of carbonaceous matter in a central Tibetan Plateau river basin. *Environmental Research* **216**. doi: 10.1016/j.envres.2022.114680

Li XY and 6 others (2015) An 80-year summer temperature history from the Xiao Dongkemadi ice core in the central Tibetan Plateau and its association with atmospheric circulation. *Journal of Asian Earth Sciences* **98,** 285-295. doi: 10.1016/j.jseaes.2014.09.025

Li YF, Huang J, Li Z and Zheng K (2020) Atmospheric pollution revealed by trace elements in recent snow from the central to the northern Tibetan Plateau. *Environmental Pollution* **263**. doi: 10.1016/j.envpol.2020.114459

Liang L, Cuo L and Liu Q (2018) The energy and mass balance of a continental glacier: Dongkemadi Glacier in central Tibetan Plateau. *Scientific Reports* **8**(1)**,** 12788. doi: 10.1038/s41598-018-31228-5

Liang LQ, Cuo L and Liu Q (2019) Mass Balance Variation and Associative Climate Drivers for the Dongkemadi Glacier in the Central Tibetan Plateau. *Journal of Geophysical Research: Atmospheres* **124**(20), 10814-10825. doi: 10.1029/2019JD030615

Liang LQ, Cuo L and Liu Q (2020) Long-term temporal-scale-dependent warming effects on the mass balance in the Dongkemadi Glacier, Tibetan Plateau. *Journal of Geophysical Research: Atmospheres* **125**(20), e2020JD033105. doi: 10.1029/2020JD033105

Liang LQ, Cuo L and Liu Q (2022) The Role of the Snow Ratio in Mass Balance Change under a Warming Climate for the Dongkemadi Glacier, Tibetan Plateau. *Journal of Climate* **35,** 3833-3844. doi: 10.1175/jcli-d-21-0762.1

Liu SY, Sun WX, Shen YP and Li G (2003) Glacier changes since the Little Ice Age

maximum in the western Qilian Shan, northwest China, and consequences of glacier runoff for water supply. *Journal of Glaciology* **49**(164)**,** 117-124. doi: 10.3189/172756503781830926

Ma LL, Tian LD, Wei Y and Wei T (2008) Measuring the Depth of Gurenhekou Glacier in the South of the Tibetan Plateau Using GPR and Estimating Its Volume Based on the Outcomes. *Journal of Glaciology and Geocryology* **30**(5)**,** 783-788 (in Chinese). doi: 10.7522/j.issn.1000–0240(2008)05–0783–06

Matthews HD and Wynes S (2022) Current global efforts are insufficient to limit warming to 1.5°C. *Science* **376**(6600)**,** 1404-1409. doi: 10.1126/science.abo3378

Millan R, Mouginot J, Rabatel A and Morlighem M (2022) Ice velocity and thickness of the world's glaciers. *Nature Geoscience* **15**(2)**,** 124-129. doi: 10.1038/s41561-021-00885-z

Nuth C and Kääb A (2011) Co-registration and bias corrections of satellite elevation data sets for quantifying glacier thickness change. *The Cryosphere* **5**(1)**,** 271-290. doi: 10.5194/tc-5-271-2011

Oerlemans J (2005) Extracting a climate signal from 169 glacier records. *Science* **308**(5722)**,** 675-677. doi: 10.1126/science.1107046

Oerlemans J and Reichert BK (2000) Relating glacier mass balance to meteorological data by using a seasonal sensitivity characteristic. *Journal of Glaciology* **46**(152)**,** 1-6. doi: 10.3189/172756500781833269

Paudyal R and 9 others (2017) Insights into mercury deposition and spatiotemporal variation in the glacier and melt water from the central Tibetan Plateau. *Science of the Total Environment* **599-600,** 2046-2053. doi: 10.1016/j.scitotenv.2017.05.145

Paul F and 19 others (2013) On the accuracy of glacier outlines derived from

remote-sensing data. *Annals of Glaciology* **54**(63)**,** 171-182. doi: 10.3189/2013AoG63A296

Pritchard HD (2019) Asia's shrinking glaciers protect large populations from drought stress. *Nature* **569**(7758)**,** 649-654. doi: 10.1038/s41586-019-1240-1

Pritchard HD, King EC, Goodger DJ, McCarthy M, Mayer C and Kayastha R (2020) Towards Bedmap Himalayas: development of an airborne ice-sounding radar for glacier thickness surveys in High-Mountain Asia. *Annals of Glaciology* **61**(81)**,** 35-45. doi: 10.1017/aog.2020.29

Pu JC and 6 others (2008) Rapid decrease of mass balance observed in the Xiao (Lesser) Dongkemadi Glacier, in the central Tibetan Plateau. *Hydrological Processes* **22**(16)**,** 2953-2958. doi: 10.1002/hyp.6865

Rounce DR, Hock R and Shean DE (2020) Glacier Mass Change in High Mountain Asia Through 2100 Using the Open-Source Python Glacier Evolution Model (PyGEM). *Frontiers in Earth Science* **7**. doi: 10.3389/feart.2019.00331

Schroeder DM and 9 others (2020) Five decades of radioglaciology. *Annals of Glaciology* **61**(81)**,** 1-13. doi: 10.1017/aog.2020.11

Shangguan DH, Liu SY, Ding YJ, Zhang YS, Du EJ and Wu Z (2008) Thinning and retreat of Xiao Dongkemadi glacier, Tibetan Plateau, since 1993. *Journal of Glaciology* **54**(188)**,** 949-951. doi: 10.3189/002214308787780003

Shean DE and 6 others (2016) An automated, open-source pipeline for mass production of digital elevation models (DEMs) from very-high-resolution commercial stereo satellite imagery. *Isprs Journal of Photogrammetry and Remote Sensing* **116,** 101-117. doi: 10.1016/j.isprsjprs.2016.03.012

Shean DE, Bhushan S, Montesano P, Rounce DR, Arendt A and Osmanoglu B (2020) A Systematic, Regional Assessment of High Mountain Asia Glacier Mass

Balance. *Frontiers in Earth Science* **7,** 363. doi: 10.3389/feart.2019.00363

Shi PH, Duan KQ, Nicholson KN, Han BS, Klaus N and Yang JH (2020) Modeling past and future variation of glaciers in the Dongkemadi Ice Field on central Tibetan Plateau from 1989 to 2050. *Arctic Antarctic and Alpine Research* **52**(1)**,** 191-209. doi: 10.1080/15230430.2020.1743157

Shi PH, Duan KQ, Liu HC, Yang JH, Zhang X and Sun JY (2016) Response of Xiao Dongkemadi Glacier in the central Tibetan Plateau to the current climate change and future scenarios by 2050. *Journal of Mountain Science* **13**(1)**,** 13-28. doi: 10.1007/s11629-015-3609-4

Thibert E, Blanc R, Vincent C and Eckert N (2008) Glaciological and volumetric mass-balance measurements: error analysis over 51 years for Glacier de Sarennes, French Alps. *Journal of Glaciology* **54**(186)**,** 522-532. doi: 10.3189/002214308785837093

Tian LD, Masson-Delmotte V, Stievenard M, Yao TD and Jouzel J (2001) Tibetan Plateau summer monsoon northward extent revealed by measurements of water stable isotopes. *Journal of Geophysical Research-Atmospheres* **106**(D22)**,** 28081-28088. doi: 10.1029/2001jd900186

Wang NL, He JQ, Pu JC, Jiang X and Jing ZF (2010) Variations in equilibrium line altitude of the Qiyi Glacier, Qilian Mountains, over the past 50 years. *Chinese Science Bulletin* **55**(33)**,** 3810-3817. doi: 10.1007/s11434-010-4167-3

Wang NL and Pu JC (2009) Ice Thickness, Sounded by Ground Penetrating Radar, on the Bayi Glacier in the Qilian Mountains, China. *Journal of Glaciology and Geocryology* **31**(3)**,** 431-435 (in Chinese). doi: 10.7522/j.issn.1000–0240(2009)03–0431–05

Wang S, Yao TD, Tian LD and Pu JC (2017) Glacier mass variation and its effect on surface runoff in the Beida River catchment during 1957-2013. *Journal of Glaciology* **63**(239)**,** 523-534. doi: 10.1017/jog.2017.13

Welty E and GlaThiDa Contributors (2020) Worldwide version-controlled database of glacier thickness observations. *Earth System Science Data* **12**(4)**,** 3039-3055. doi: 10.5194/essd-12-3039-2020

WGMS (2021) *Global Glacier Change Bulletin No. 4 (2018–2019)*. Zurich, Switzerland: ISC(WDS)/IUGG(IACS)/UNEP/UNESCO/WMO, World Glacier Monitoring Service. doi: 10.5904/wgms-fog-2021-05

Wu KP and 8 others (2021) Quantification of glacier mass budgets in the Karakoram region of Upper Indus Basin during the early twenty-first century. *Journal of Hydrology* **603,** 127095. doi: 10.1016/j.jhydrol.2021.127095

Wu XJ, Wang NL, Lu AX, Pu JC, Guo ZM and Zhang HW (2015) Variations in albedo on Dongkemadi Glacier in Tanggula Range on the Tibetan Plateau during 2002-2012 and its linkage with mass balance. *Arctic Antarctic and Alpine Research* **47**(2)**,** 281-292. doi: 10.1657/aaar00c-13-307

Wu Z, Liu SY and He XB (2016) Numerical simulation of the flow velocity and temperature of the Dongkemadi Glacier. *Environmental Earth Sciences* **75**(5). doi: 10.1007/s12665-016-5262-9

Xie J, Wang NL, Pu JC and Chen L (2009) Study of the Bacterial Diversity Recovered from Glacial Snow of the Northern Tibetan Plateau. *Journal of Glaciology and Geocryology* **31**(2)**,** 342-349 (in Chinese). doi: 10.7522/j.issn.1000–0240(2009)02–0342–08

Xu CH, Li ZQ, Li HL, Wang FT and Zhou P (2019) Long-range terrestrial laser

scanning measurements of annual and intra-annual mass balances for Urumqi Glacier No. 1, eastern Tien Shan, China. *The Cryosphere* **13**(9)**,** 2361-2383. doi: 10.5194/tc-13-2361-2019

Yang W, Yao TD, Guo XF, Zhu ML, Li SH and Kattel DB (2013) Mass balance of a maritime glacier on the southeast Tibetan Plateau and its climatic sensitivity. *Journal of Geophysical Research-Atmospheres* **118**(17)**,** 9579-9594. doi: 10.1002/jgrd.50760

Yao TD and 15 others (2022) The imbalance of the Asian water tower. *Nature Reviews Earth & Environment* **3**(10)**,** 618-632. doi: 10.1038/s43017-022-00299-4

Yao TD and 13 others (2013) A review of climatic controls on δ18O in precipitation over the Tibetan Plateau: Observations and simulations. *Reviews of Geophysics* **51**(4), **525-548**. doi:10.1002/rog.20023

Yao TD and 14 others (2012) Different glacier status with atmospheric circulations in Tibetan Plateau and surroundings. *Nature Climate Change* **2**(9)**,** 663-667. doi: 10.1038/nclimate1580

Zemp M and 14 others (2020) Global glacier mass changes and their contributions to sea-level rise from 1961 to 2016 (vol 568, pg 382, 2019). *Nature* **577**(7792)**,** 382-386. doi: 10.1038/s41586-019-1889-5

Zemp M and 16 others (2013) Reanalysing glacier mass balance measurement series. *The Cryosphere* **7**(4)**,** 1227-1245. doi: 10.5194/tc-7-1227-2013

Zhang GF, Li ZQ, Wang WB and Wang WD (2014) Rapid decrease of observed mass balance in the Urumqi Glacier No. 1, Tianshan Mountains, central Asia. *Quaternary International* **349,** 135-141. doi: 10.1016/j.quaint.2013.08.035

Zhang J, He XB, Ye BS and Wu JK (2013) Recent Variation of Mass Balance of the

Xiao Dongkemadi Glacier in the Tanggula Range and Its Influencing Factors. *Journal of Glaciology and Geocryology* **35**(2)**,** 263-271 (in Chinese). doi: 10.7522/j.issn.1000–0240.2013.0032

Zhang Y (2023) Glacier Change in Tanggula Mountain and Its Response to Climate Fluctuation from 1980 to 2020. Liaoning Normal University (in Chinese).

Zhang ZM, Jiang LM, Liu L, Sun YF and Wang HS (2018) Annual Glacier-Wide Mass Balance (2000-2016) of the Interior Tibetan Plateau Reconstructed from MODIS Albedo Products. *Remote Sensing* **10**(7)**,** 1031. doi: 10.3390/rs10071031

Zhou YS, Li ZW, Li J, Zhao R and Ding XL (2018) Glacier mass balance in the Qinghai Tibet Plateau and its surroundings from the mid-1970s to 2000 based on Hexagon KH-9 and SRTM DEMs. *Remote Sensing of Environment* **210,** 96-112. doi: 10.1016/j.rse.2018.03.020

Zhu ML, Yao TD, Yang W and Tian LD (2014) Ice volume and characteristics of sub-glacial topography of the Zhadang Glacier, Nyainqentanglha Range. *Journal of Glaciology and Geocryology* **36**(2)**,** 268-277(in Chinese). doi: 10.7522/j.issn.1000–0240

Table 1. Details of multi–source remote sensing data.

Source	Date Acquired*	ID	Spatial resolution	Application
Topographic map	—/11/1969*	—**	1:100,000	Area and DEM
SRTM	—/02/2000*	SRTM3N33E092V1	90 m	DEM
Landsat TM	13/04/1999	LT05_L1TP_138037_19990413_20200908_02_T1	30 m	Area
Landsat OLI	30/12/2015	LC08_L1TP_137037_20151230_20200908_02_T1	15 m	Area
Landsat OLI	27/12/2020	LC08_L1TP_137037_20201227_20210310_02_T1	15 m	Area
ASTER	29/12/2015	L1A_00312292015044606	15 m	Area and DEM
ZY –3	09/10/2020	ZY303_TMS_E92.2_N33.1_20201009_L1A0000063138	2.1 m/3.5 m***	Area and DEM

Note: *Date acquired given in dd/mm/yyyy format, noting that the specific dates for the Topographic map and SRTM were unavailable. **The ID of topographic map is confidential. ***The spatial resolutions of the orthophotos and stereopsis are 2.1 and 3.5 m, respectively.

Table 2. Changes in area, surface elevation, and geodetic mass balance of XDG during the 1969–2020.

Time	Glacier area (km^2)	Period	Area change		Geodetic mass budgets	
			km^2	$\%\cdot a^{-1}$	MED (m a^{-1})	SMB (m w.e. a^{-1})
1969	1.77±0.08	1969–1999	– 0.10±0.15	– 0.19±0.28	– 0.07±0.12	–0.06±0.10

https://doi.org/10.1017/jog.2024.100 Published online by Cambridge University Press

1999	1.67±0.13	1999–2015	–0.17±0.14	–0.64±0.52	–0.48±0.23	–0.41±0.14
2015	1.50±0.06	2015–2020	–0.02±0.06	–0.27±0.83	–0.36±0.43	–0.32±0.14
2020	1.48±0.02	1969–2020	–0.29±0.08	–0.32±0.09	–0.23±0.07	–0.19±0.02

Note: The geodetic results for the period before 2015 are sourced from Chen and others (2017), but the mass balance uncertainty is estimated using a new equation presented in this study, MED denotes the mean elevation difference; and SMB stands for specific mass balance.

Table 3. Changes in mean ice thickness and ice volume of XDG during the 1969–2020.

Time	Mean ice thickness (m)	Ice volume (km^3)	Period	Ice volume change	
				km^3	$\%\cdot a^{-1}$
1969	66.40±3.44	0.1175±0.0066	1969-2000	- 0.0102±0.0064	- 0.29±0.18
1999	64.28±3.73	0.1073±0.0104	2000-2015	- 0.0225±0.0063	- 1.00±0.37
2015	56.56±2.13	0.0848±0.0047	2015-2020	- 0.0038±0.0032	- 0.89±0.75
2020	54.78±3.69	0.0811±0.0056	1969-2020	- 0.0364±0.0051	- 0.61±0.09

Note: The uncertainty of the mean ice thickness in 2020 was estimated from GPR measurements, and the other uncertainties were based on via geodetic method.

https://doi.org/10.1017/jog.2024.100 Published online by Cambridge University Press

Table 4. Correlation coefficients between the XDG mass balance, and temperature and precipitation at Anduo meteorological station for different seasonal periods.

Period	Temperature	Precipitation
Annual	–0.39*	0.42*
Cold season	–0.15	–0.02
Warm season	–0.79**	0.43*
Summer	–0.79**	0.27
Winter	–0.15	0.22

Note: ** significant correlation with less than 0.01 probability of random chance for the relationship, * significant correlation with less than 0.05 probability of random chance for the relationship.

Table 5. Mass balance values for XDG and DG during different periods, as obtained from the glaciological method and Hugonnet and others (2021).

Periods	glaciological values (m w.e. a^{-1})	Hugonnet et al.'s values (m w.e. a^{-1})
2000-2005	-0.20	-0.17 ± 0.45
2005-2010	-0.37	-0.31 ± 0.40
2010-2015	-0.50	-0.62 ± 0.35
2015-2020	--	-0.87±0.46
2000-2010	-0.29	-0.23±0.21

https://doi.org/10.1017/jog.2024.100 Published online by Cambridge University Press

Figure Captions

Fig. 1. Location of XDG. (a) Geographical location of Dongkemadi Ice Field in the Tibetan Plateau, with the red star is the location of Anduo meteorological station; (b) location of XDG in the Dongkemadi Ice Field; (c) stake network on XDG in 2015.

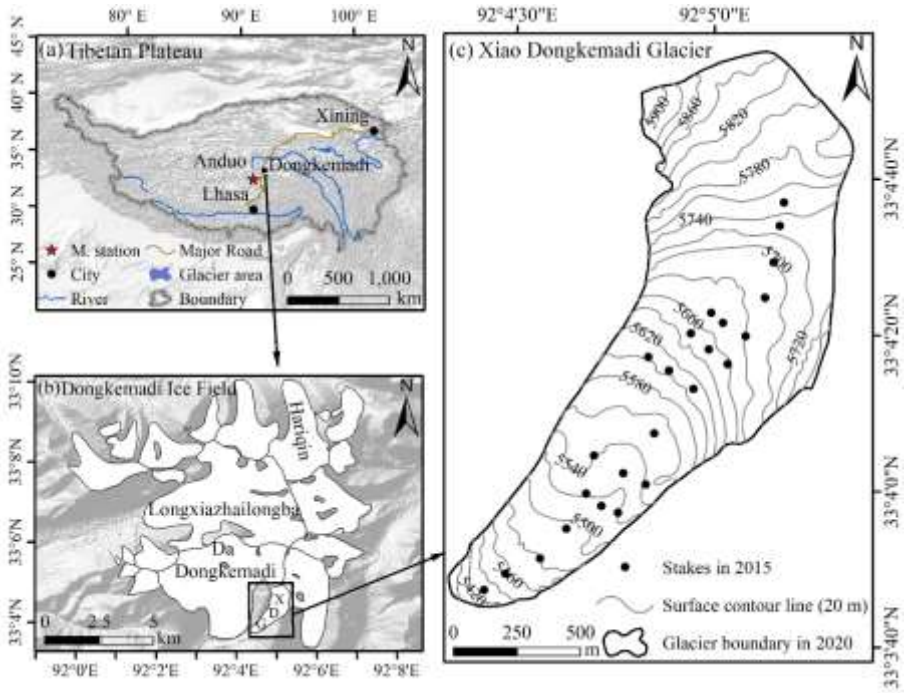

Fig. 2. GPR measurements on XDG: (a) distribution of GPR measurement points; (b) GPR profile along transect AA' in (a).

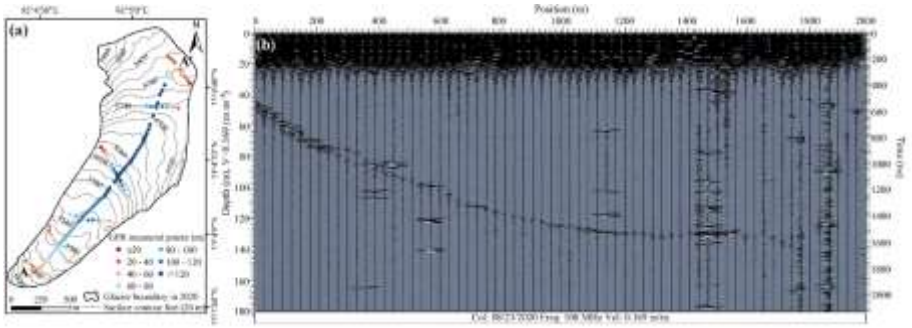

https://doi.org/10.1017/jog.2024.100 Published online by Cambridge University Press

Fig. 3. Cross–validation of the Ordinary Kriging method: (a) distribution of the verification points; (b) comparison between interpolated and measured ice–thickness values.

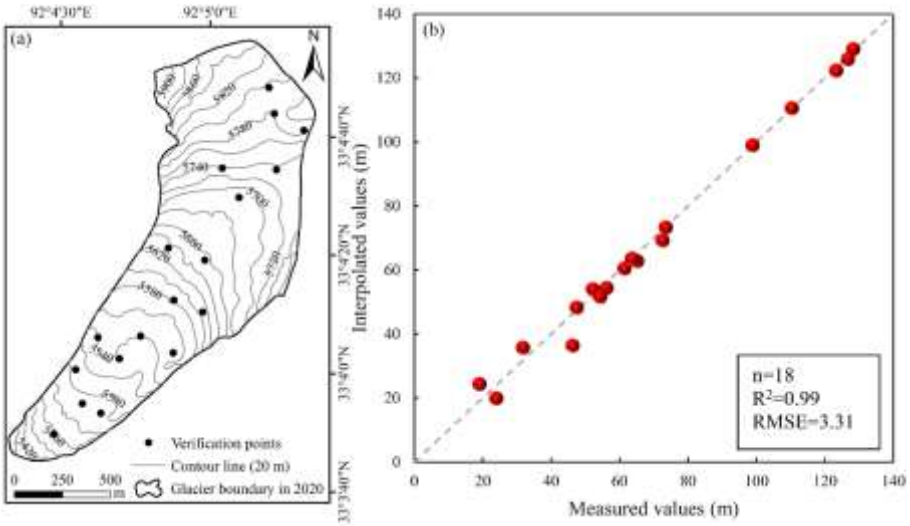

Fig. 4. Variations in warm season temperature (red) and precipitation (blue) at the median height (5600 m a.s.l.) of XDG from 1967 to 2020.

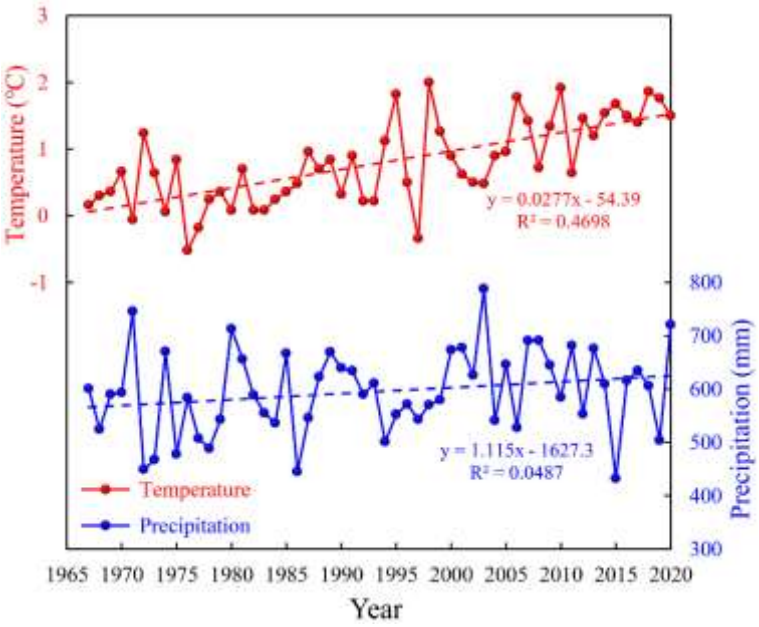

https://doi.org/10.1017/jog.2024.100 Published online by Cambridge University Press

Fig. 5. Annual glaciological mass balance (blue), cumulative mass balance (red), mean glaciological value for 1999-2015 (yellow line), and annual rate of geodetic mass balances (black lines, with the orange regions indicating the uncertainty of geodetic results) of XDG over the investigated periods, 5-yearly geodetic mass balances (purple lines, with the light blue regions indicating the uncertainty of geodetic results) provided by Hugonnet and others (2021) for DG.

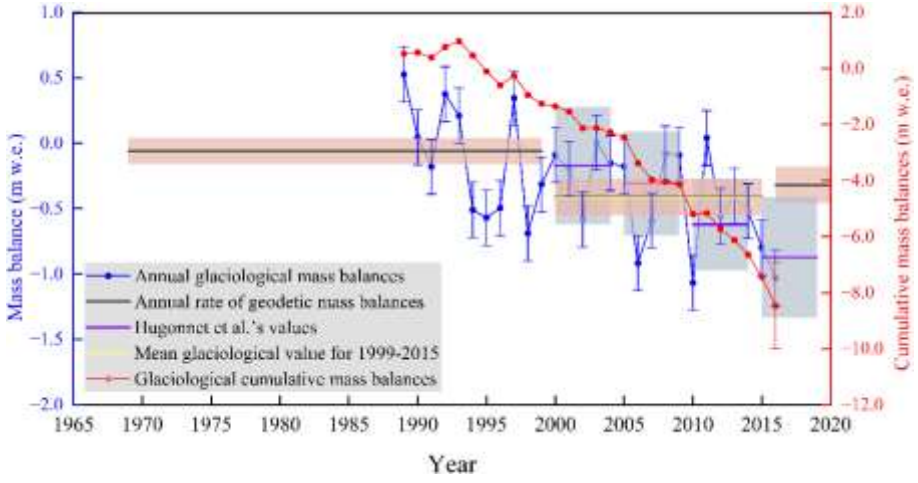

https://doi.org/10.1017/jog.2024.100 Published online by Cambridge University Press

Fig. 6. XDG boundaries in 1969 (red, derived from a topographic map); 1999 (yellow, derived from Landsat 5 satellite imagery); 2015 (purple, derived from Landsat 8 satellite imagery); and 2020 (blue, derived from ZY–3 satellite imagery). The background image is a ZY–3 satellite imagery acquired on 9 October, 2020. The dashed circle highlights an area of extensive surface lowering along the western headwall of XDG.

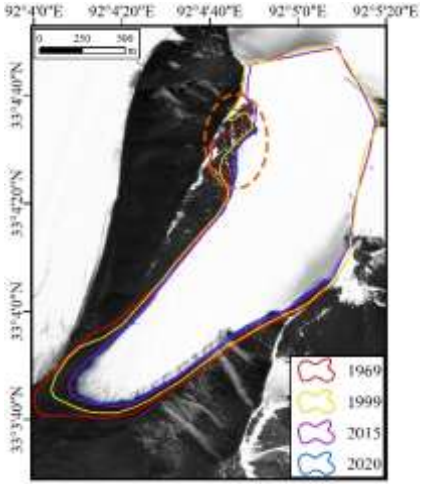

Fig. 7. Glacier thickness in 2020 (a) and morphology of ice bed (b) for XDG.

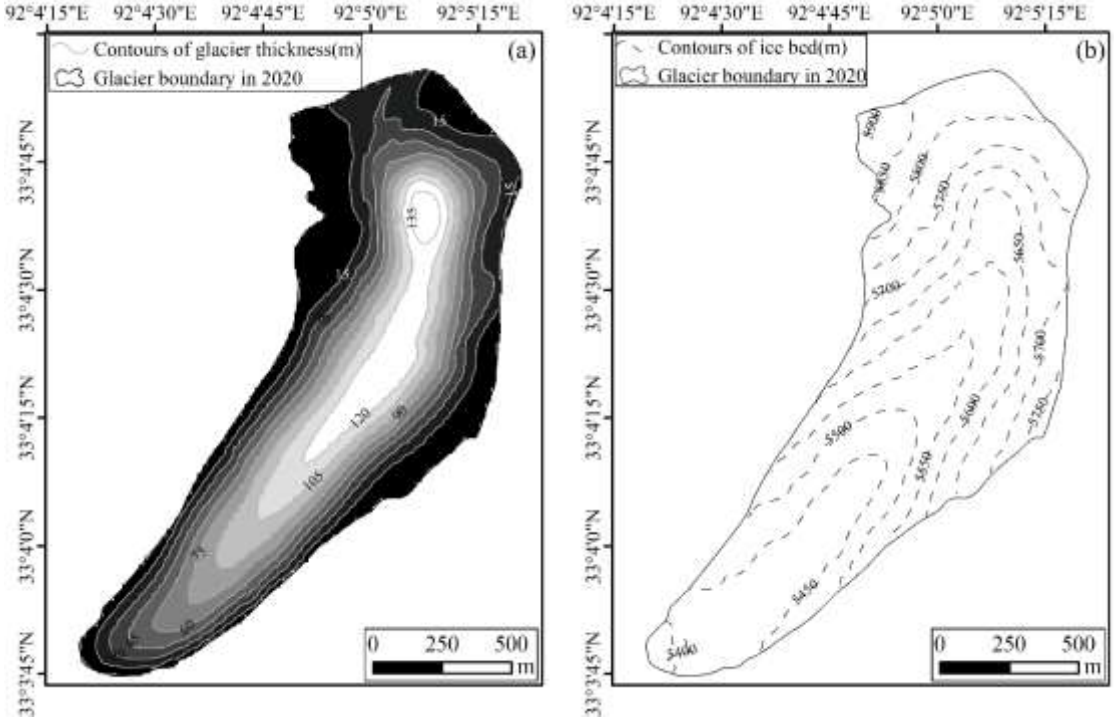

https://doi.org/10.1017/jog.2024.100 Published online by Cambridge University Press

Fig. 8. XDG surface-elevation differences for the (a) 1969–1999, (b) 1999–2015, and (c) 2015–2020 periods.

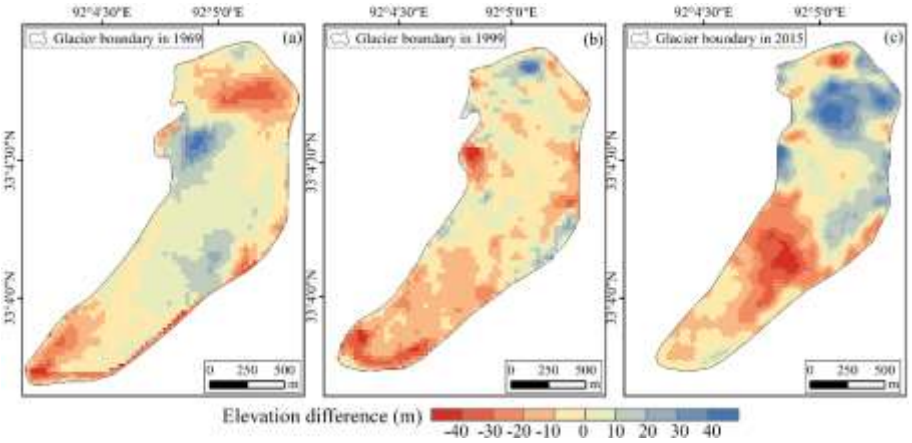

Fig. 9. Variations in the mass balance of XDG from 1967 to 2020 are illustrated as follows: (a) Triangles denote observed values (black), closed circles represent reconstructed values (blue), and the reconstructed cumulative mass balance is shown in red; (b) comparison between observed and reconstructed values.

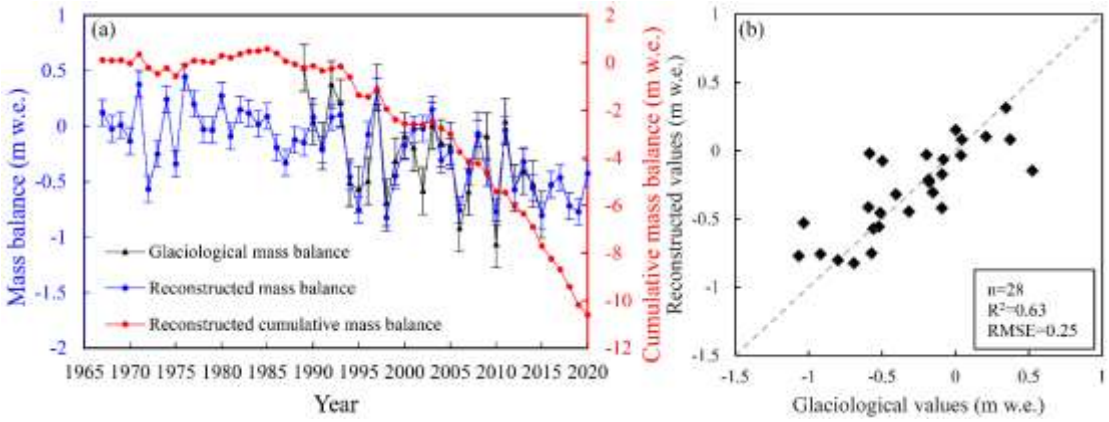

https://doi.org/10.1017/jog.2024.100 Published online by Cambridge University Press

Fig. 10. Comparison of annual mass balance between glaciological method for XDG and those provided by Hugonnet and others (2021) for DG.

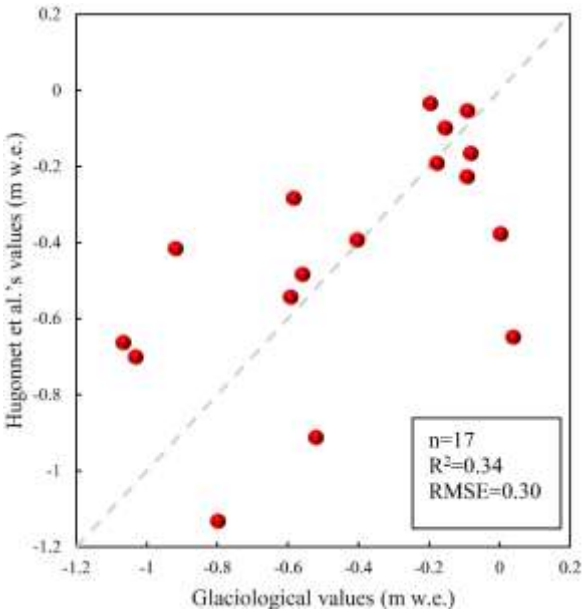

Fig. 11. The distribution of glacier thickness for XDG in 1999 (a) reconstructed values of this study, (b) estimated values released by Farinotti and others (2019).

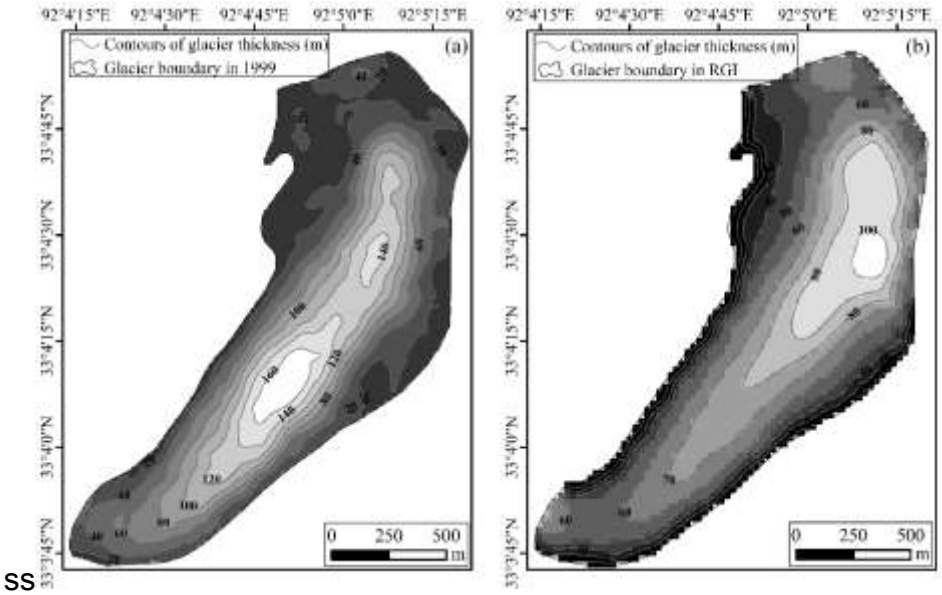

SS

https://doi.org/10.1017/jog.2024.100 Published online by Cambridge University Press